Ground State Analysis of the Spin-1/2 XX Chain Model with Anisotropic Three-Spin Interaction

N. Mahboob[1], S. Mahdavifar[1],* and F. Khastehdel Fumani[2]
[1] *Department of Physics, University of Guilan, 41335-1914, Rasht, Iran and*
[2] *Department of Basic Sciences, Langarud Branch, Islamic Azad University, Langarud, Iran*

In this paper, we investigate the ground state properties of the spin-1/2 XX chain model with anisotropic three-spin interaction using the fermionization technique. By exactly diagonalizing the Hamiltonian, we analyze the dispersion relation, ground state energy, fidelity susceptibility, and order parameters. Our results reveal two gapless phases separated by a second-order critical line: a composite phase exhibiting both chiral and spin-nematic-I long-range orderings, and a phase characterized by spin-nematic-II long-range ordering.

Further, we study the ground state phase diagram through the concurrence and quantum discord between nearest-neighbor spins, finding that these measures are maximized at the critical line, with an additional entangled region observed. Finally, we examine the spin squeezing parameter and entanglement entropy, demonstrating that the ground state is squeezed throughout and becomes extremely squeezed at the critical line. Notably, in the gapless spin-nematic-II phase, the Heisenberg limit is achieved. By dividing the system into two equal parts, we observe significant entanglement in the gapless composite phase. The central charge calculation confirms the critical nature of the gapless spin-nematic-II phase, while the entanglement entropy follows volume-law scaling in the gapless composite phase.

I. INTRODUCTION

The quantum ground state represents the lowest energy configuration of a quantum mechanical system, where all particles occupy the minimum available energy levels. Also known as the zero-point energy state, it signifies the least amount of energy a system can possess, even at absolute zero temperature. The ground state phase describes the characteristics and behavior of a system in this minimal energy state. Grasping the ground state phase is essential for exploring quantum phenomena, particularly in low-dimensional quantum magnets [1 and 2].

A ground state phase diagram maps out the different phases of a quantum system at its lowest energy state as various parameters, such as pressure, or magnetic field, are varied [3 and 4]. This diagram is crucial for understanding quantum phenomena, predicting material properties, and exploring quantum phase transitions, which occur at absolute zero temperature and are driven by quantum fluctuations. Its applications span material science, where it aids in designing new materials like superconductors and magnetic materials, quantum computing, where it helps optimize quantum algorithms and understand qubit behavior, and condensed matter physics, where it is essential for studying phenomena such as superconductivity, magnetism, and topological phases of matter.

There are several types of quantum phase transitions. A gapped-gapped phase transition occurs between two distinct phases of a quantum system, both of which have an energy gap between the ground state and the first excited state. This transition is characterized by a change in the system's properties without closing the energy gap. In spin-1/2 chains, the transition between different topological phases, such as the Haldane phase, is a well-known example [5]. The Haldane phase is a gapped phase with unique topological properties and edge states.

A gapped-gapless phase transition occurs when a quantum system transitions from a phase with an energy gap to a phase without an energy gap. This type of transition is significant because it often involves changes in the system's symmetry and topological properties. In the one-dimensional XXZ spin-1/2 chain, tuning the anisotropy parameter can lead to a transition from a gapped phase to a gapless Luttinger liquid phase [6–8].

A gapless-gapless phase transition refers to a transition between two different gapless phases in a quantum system. In these transitions, the system remains gapless before and after the transition, but the nature of the gapless excitations changes. In spin-1/2 chain systems the three-spin interaction (TSI) can induce a gapless-gapless quantum phase transition. This is a type of cluster interaction, where a group of spins interact collectively. In particular, TSI is when three spins are coupled by a term that depends on the product of their spin components. TSI can cause frustration, entanglement, and quantum phase transitions in spin systems. Two different type of TSI are well known. The Hamiltonian of the first model is given by

$$\mathcal{H} = J^{'} \sum_{n=1}^{N} [\left(S_n^x S_{n+2}^x + S_n^y S_{n+2}^y\right) \ S_{n+1}^z], \tag{1}$$

where S_n is the spin operator at the n-th site and $J^{'}$ denotes the strength of the TSI. The impact of this type of TSI on the spin-1/2 Heisenberg chain model has been extensively studied [9–27]. Notably, when this interaction is added to the spin-1/2 XX chain model, it induces

* smahdavifar@gmail.com

a gapless-gapless quantum phase transition [10].

The Hamiltonian of the second model is expressed as

$$\mathcal{H} = J^{'} \sum_{n=1}^{N} \left(S_n^x S_{n+2}^y - S_n^y S_{n+2}^x \right) \ S_{n+1}^z . \tag{2}$$

The effects of this type of TSI on the spin-1/2 Heisenberg chain model are also well-documented [28–35]. Specifically, when this interaction is introduced to the spin-1/2 XX chain model, a gapless-gapless quantum phase transition is observed [29].

Studying gapless-gapless quantum phase transitions in spin-1/2 chain systems is crucial for both condensed matter physics and quantum information science. In condensed matter physics, these transitions provide deep insights into quantum criticality, where systems undergo continuous phase transitions at absolute zero temperature. This understanding helps in exploring the behavior of materials at critical points and the nature of quantum fluctuations. Additionally, these studies can reveal exotic phases of matter, such as spin liquids, which do not fit into conventional classifications and offer new perspectives on the properties of quantum materials.

From the viewpoint of quantum information and technology, gapless systems exhibit unique entanglement properties that are essential for quantum information processing, leading to advancements in quantum algorithms and error correction methods. Moreover, some gapless phases are related to topological phases, which are robust against local perturbations, making them ideal for fault-tolerant quantum computation. Understanding these transitions also aids in the design of new materials with specific quantum properties, crucial for developing advanced quantum technologies like quantum sensors and communication devices. Spin-1/2 chains serve as versatile platforms for simulating other quantum systems, thus playing a significant role in the development and testing of new quantum technologies.

Recently, there has been significant interest in studying the effects induced by anisotropic three-spin interactions (ATSI). Specially studies are focussed on the anisotropic form of the first model which is defined as

$$\mathcal{H} = J' \sum_{n=1}^{N} \left[(S_n^x S_{n+2}^x + \beta S_n^y S_{n+2}^y) \ S_{n+1}^z \right], \tag{3}$$

where β is the anisotropy parameter. Recent studies have highlighted that this kind of ATSI can induce non-trivial gapped topological phases in the ground state phase diagrams of spin-1/2 XY and XX chain models [18, 36–40]. Researchers have explored the topological characterization of extended quantum Ising models, showing that these models can be represented as loops in a two-dimensional auxiliary space, with the winding number serving as a topological quantum number for the quantum phases [18]. Additionally, investigations into pairwise entanglement and quantum discord in the XY spin model with ATSI have demonstrated how the anisotropic parameter affects quantum correlations at both zero and finite temperatures [36]. Further research has examined the decoherence and relaxation dynamics of topological states in extended quantum Ising models, using the Lindblad equation to analyze dephasing rates between different degenerate ground states in the topological phase at low temperatures [37]. It has also been proposed that the behaviors of long-range, two-site quantum resources can diagnose quantum phases in an XX spin chain, revealing that quantum coherence and quantum discord behaviors can signify topological quantum phases and potentially have applications in quantum information processing [38].

In this study, we investigate the ground state of the spin-1/2 XX chain model with the second type of ATSI, described by the Hamiltonian:

$$\mathcal{H} = J' \sum_{n=1}^{N} \left[(S_n^x S_{n+2}^y + \beta S_n^y S_{n+2}^x) S_{n+1}^z \right] . \tag{4}$$

Our goal is to provide a comprehensive depiction of the ground state phase diagram using tools from both condensed matter physics, quantum information science and quantum measurements. Using the fermionization technique, the exact ground state is obtained. Initially, by analyzing the dispersion relation, ground state energy, fidelity susceptibility, and cluster order parameters, two gapless phases separated by a second-order critical line are identified: a composite phase with chiral and spin-nematic-I long-range orderings, and a phase with spin-nematic-II long-range ordering. Next, by examining the concurrence and quantum discord (QD) between nearest-neighbor spins, the ground state phase diagram is studied, revealing that these functions are maximized on the critical line and an entangled region is observed. Finally, the ground state phase diagram is analyzed using the spin squeezing parameter and entanglement entropy (EE). Results show that the ground state is squeezed throughout and becomes extremely squeezed at the critical line. Surprisingly, in the gapless spin-nematic-II phase, the Heisenberg limit is achieved. Dividing the system into two equal parts reveals high entanglement in the gapless composite phase. The central charge is calculated, showing that the gapless spin-nematic-II phase is critical based on EE scaling, and EE follows volume-law scaling in the gapless composite phase.

The structure of the paper is as follows: In the next section, we introduce the model and determine the ground state using the fermionization technique. Section III presents the results. Finally, Section IV concludes with our findings.

II. THE MODEL

The Hamiltonian of the 1D spin-1/2 XX model with ATSI is denoted as

$$\mathcal{H} = J\sum_{n=1}^{N}\left[S_n^x S_{n+1}^x + S_n^y S_{n+1}^y\right] + J'\sum_{n=1}^{N}\left[\left(S_n^x S_{n+2}^y + \beta S_n^y S_{n+2}^x\right) S_{n+1}^z\right], \qquad (5)$$

where symbol $J > 0$ represents the antiferromagnetic exchange coupling. The variable N denotes the size of the system, which corresponds to the number of spins. We are assuming the periodic boundary condition, denoted as $S_{n+N}^\mu = S_n^\mu$, where μ might take the directions of x, y, or z. Assuming $\alpha = \frac{J'}{J}$ is considered valid and does not affect the generality of the situation.

A. Symmetry Arguments

Consider a unitary transformation defined as $U_z = \prod_{n=1}^{N} e^{i\pi n S_n^z}$, which results in the following transformations:

$$S_n^{x,y} \longrightarrow (-1)^n S_n^{x,y}, \quad S_n^z \longrightarrow S_n^z. \qquad (6)$$

When N is even, the Hamiltonian satisfies the symmetry relation:

$$U_z \mathcal{H}(J, J', \beta) U_z^\dagger = \mathcal{H}(-J, J', \beta), \qquad (7)$$

indicating that the system's features for $J < 0$ can be reconstructed using this transformation. Additionally, by time reversal transformation, τ, we obtain:

$$\tau \mathcal{H}(J, J', \beta)\tau^\dagger = \mathcal{H}(J, -J', \beta), \qquad (8)$$

allowing the properties of the system for $J' < 0$ to be derived from the ground state phase diagram for $J' > 0$. Finally, under the combined symmetry operator $W = \tau\, U_z$, the Hamiltonian transforms as:

$$W\mathcal{H}(J, J', \beta)W^\dagger = -\mathcal{H}(J, J', \beta), \qquad (9)$$

which implies that the energy spectrum of the Hamiltonian exhibits inversion symmetry around zero energy, reflecting a particle-hole-like symmetry. This further suggests that zero-energy states must appear in pairs if present in the spectrum.

Therefore the ATSI disrupts several symmetries in the pure 1D spin-1/2 XX model, specifically:

* The $U(1)$ symmetry,

* Time reversal symmetry,

* The parity symmetry.

In the rest of this paper we show that the breaking of $U(1)$ symmetry, time reversal symmetry, and parity symmetry in the spin-1/2 XX chain model with ATSI significantly influences the ground state properties and phase behaviors. The $U(1)$ symmetry breaking leads to the emergence of chiral and spin-nematic-I long-range orderings, enhancing quantum correlations such as concurrence and quantum discord. Time reversal symmetry breaking is directly related to the presence of chiral order and influences the critical behavior, enhancing quantum correlations at the critical line. Parity symmetry breaking contributes to the unique long-range ordering in the spin-nematic-II phase and affects entanglement properties and spin squeezing, leading to enhanced quantum correlations and squeezing.

Overall, the interplay between these symmetry breakings and the anisotropic three-spin interaction results in a rich tapestry of ground state properties, including distinct gapless phases, critical lines, and regions of enhanced quantum correlations. These findings provide valuable insights into quantum phase transitions and the role of multi-spin interactions in low-dimensional quantum systems, with potential implications for the development of quantum technologies.

B. Diagonalization

The Hamiltonian (Eq. (5)) can be exactly diagonalized using the fermionization approach. By applying the Jordan-Wigner transformation as follows:

$$S_n^+ = a_n^\dagger e^{i\pi\left(\sum_{l<n} a_l^\dagger a_l\right)}, \quad S_n^z = a_n^\dagger a_n - \frac{1}{2}, \qquad (10)$$

where $a_n^\dagger$ and a_n are the fermionic operators, the fermionized noninteracting form of the Hamiltonian is obtained as:

$$\mathcal{H} = \frac{J}{2}\sum_{n=1}^{N}(a_n^\dagger a_{n+1} + a_{n+1}^\dagger a_n) + \frac{i}{8}\alpha(\beta - 1)\sum_{n=1}^{N}(a_n^\dagger a_{n+2} - a_{n+2}^\dagger a_n) + \frac{i}{8}\alpha(\beta + 1)\sum_{n=1}^{N}(a_n^\dagger a_{n+2}^\dagger - a_{n+2} a_n). \qquad (11)$$

By performing a Fourier transformation as $a_n = \frac{1}{\sqrt{N}}\sum_k e^{-ikn} a_k$, and also a Bogoliubov transformation:

$$a_k = \cos(\theta_k)\gamma_k - \sin(\theta_k)\gamma_{-k}^\dagger, \qquad (12)$$

the diagonalized Hamiltonian is obtained as:

$$\mathcal{H} = \sum_{k=-\pi}^{\pi} \varepsilon(k)(\gamma_k^\dagger \gamma_k - \frac{1}{2}). \qquad (13)$$

The single-particle dispersion relation or the energy spectrum is given by:

$$\varepsilon(k) = \sqrt{\mathcal{A}_k^2 + \mathcal{C}_k^2} + \mathcal{B}_k, \tag{14}$$

with:

$$\begin{aligned}
\mathcal{A}_k &= J\cos(k), \\
\mathcal{B}_k &= \frac{1}{4}\alpha(\beta-1)\sin(2k), \\
\mathcal{C}_k &= \frac{1}{4}\alpha(\beta+1)\sin(2k), \\
\tan(2\theta_k) &= \frac{\mathcal{C}_k}{\mathcal{A}_k}.
\end{aligned} \tag{15}$$

In the thermodynamic limit, $N \to \infty$, the ground state of the system corresponds to the configuration where all the states with $\varepsilon(k) \leq 0$ are filled and those with $\varepsilon(k) > 0$ are empty.

For $\beta > 0$, there are only two Fermi points located at

$$K_F = \pm\pi,$$

and the ground state is the vacuum state. In the region where $\beta < 0$, if $-\beta \leq \frac{1}{\alpha^2}$, two additional Fermi points emerge at

$$\begin{aligned}
K_F^+ &= \arcsin\left(\frac{1}{\alpha\sqrt{\beta}}\right), \\
K_F^- &= -\pi + \arcsin\left(\frac{1}{\alpha\sqrt{\beta}}\right).
\end{aligned} \tag{16}$$

In this case, the ground state is characterized by all states being filled for $-\pi < K < K_F^-$ and $K_F^+ < K < \pi$. Consequently, a quantum phase transition occurs at

$$\beta_c = -\frac{1}{\alpha^2}. \tag{17}$$

This transition is between two gapless phases: one with two Fermi points and the other with four Fermi points.

III. RESULTS

A. Phase transition in the ground state

We begin our study by examining the dispersion relation, a crucial tool for investigating the microscopic properties of quantum systems and understanding quantum phase transitions. The dispersion relation describes how the energy of quasi-particles varies with their momentum, essentially mapping the distribution of energy levels as a function of the wave vector. It offers insights into the nature of elementary excitations within the system. For instance, in a gapped phase, the dispersion relation reveals a minimum energy gap, whereas in a gapless phase, it reaches zero energy at certain points. Near quantum phase transitions, the dispersion relation often exhibits critical behavior, such as the appearance of new low-energy excitations or alterations in the spectrum, signaling a transition from one phase to another.

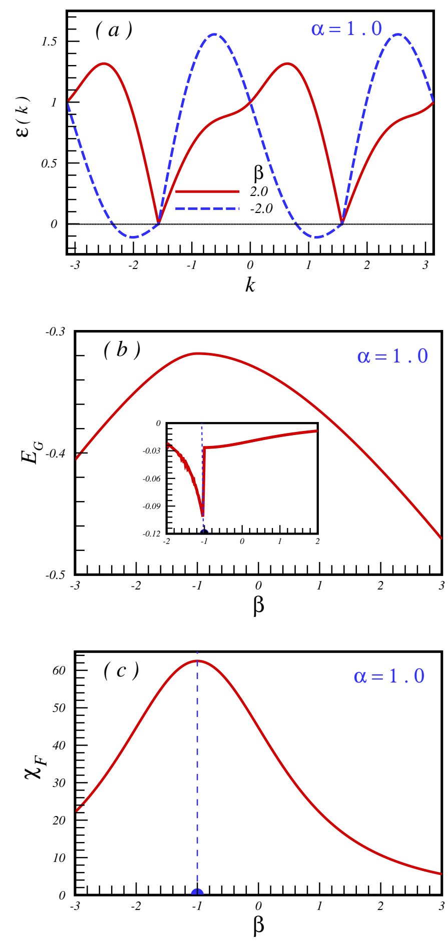

FIG. 1. (color online) (a) The spectra for various values of β and $\alpha = 1.0$ are shown for a chain system with $N = 1000$ particles. (b) The ground state energy density as a function of β at $\alpha = 1.0$ is presented, with the second derivative of the ground state energy density plotted in the inset. (c) The fidelity susceptibility as a function of β for $\alpha = 1.0$ is depicted.

In Fig. 1 (a), we have plotted $\varepsilon(k)$ as a function of k for a chain system of size $N = 1000$. We consider $\alpha = 1.0$ with two different values of $\beta = \pm 2$. The critical point in this case is $\beta_c = -1$. It is evident that there are two Fermi points when $\beta = 2 > \beta_c$ and four Fermi points when $\beta = -2 < \beta_c$. Additionally, both regions are gapless. Since there is no momentum region with $\varepsilon < 0$ for $\beta = 2 > \beta_c$, the ground state is a vacuum.

The ground-state energy density of the system is expressed as:

$$E_G = \frac{1}{2N}\sum_{k\in\Lambda}\varepsilon(k) - \frac{1}{2N}\sum_{k\notin\Lambda}\varepsilon(k), \tag{18}$$

where Λ represents the region where $\varepsilon(k) < 0$. In Fig. 1

(b), we have plotted the ground-state energy density of the system as a function of β for $\alpha = 1.0$. The inset shows the second derivative of the ground-state energy density as a function of β. It is evident that there is a discontinuity in the second derivative of the ground-state energy density, $\partial^2 E_G/\partial\beta^2$, precisely at the critical point $\beta_c = -1$, indicating a second-order quantum phase transition.

Fidelity susceptibility is a measure in quantum mechanics that quantifies the sensitivity of a quantum state to small changes in a parameter of the system's Hamiltonian. It essentially captures how much the ground state of a quantum system changes when a parameter in the Hamiltonian is varied slightly. Fidelity susceptibility is particularly useful for identifying quantum critical points because it exhibits a peak or divergence at these points. This behavior occurs because the ground state of the system changes most rapidly at the critical point, indicating a phase transition. Fidelity susceptibility is defined as [41–43]

$$\begin{aligned}\chi_F &= \frac{2[1 - F(\beta, \beta + \delta\beta)]}{(\delta\beta)^2} \\ &= \frac{1}{2}\sum_k \left(\frac{\partial}{\partial\beta}(2\theta_k)\right)^2, \end{aligned} \tag{19}$$

where $F(\beta, \beta + \delta\beta)$ is the ground-state fidelity, quantifying the overlap amplitude between the ground-state wave function at β and $\beta + \delta\beta$. We have calculated the fidelity susceptibility, and the results are presented in Fig. 1 (c) for a chain with $N = 1000$ particles. Specifically, we observe a distinct peak in fidelity susceptibility at $\beta_c = -1.0$. This observation suggests the presence of a phase transition between two distinct gapless phases.

In the realm of quantum many-body systems, response functions and specially order parameters are crucial indicators that delineate distinct ground state domains by manifesting specific types of order. These parameters are zero in disordered phases, reflecting symmetry, and become finite in ordered phases, indicating broken symmetry. The significance of order parameters extends beyond mere classification; they are instrumental in understanding the nature of quantum phase transitions. Order parameters provide valuable insights into the character and classification of these transitions, which can either unfold gradually as continuous (second-order) transitions or occur abruptly as discontinuous (first-order) transitions. By analyzing order parameters, we gain a deeper understanding of the fundamental mechanisms governing the behavior of quantum many-body systems and the intricate nature of their phase transitions.

It is important to note that this model does not induce any magnetization. Therefore, to thoroughly understand the nature of the various gapless phases within our model, we have calculated the cluster order parameters as defined.

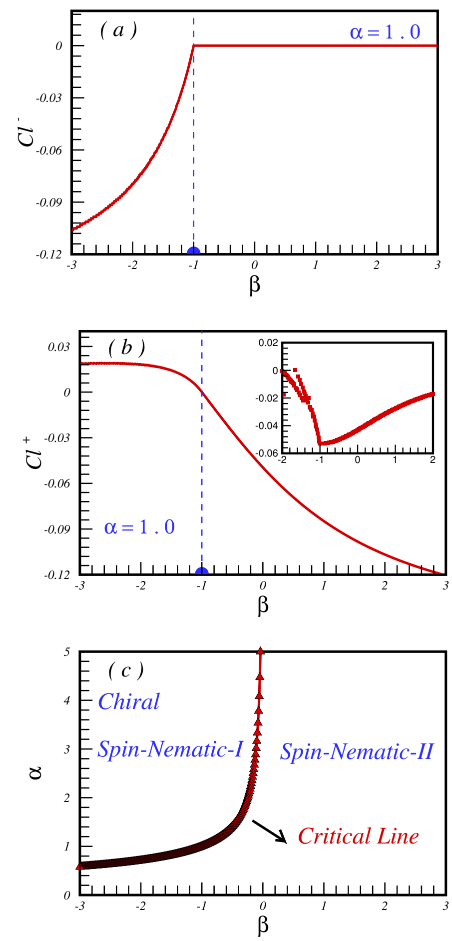

FIG. 2. (color online) The cluster order parameters (a) Cl^- and (b) Cl^+ as functions of β at $\alpha = 1.0$ for a chain system with $N = 1000$ particles. In the inset of (b), results for the first derivative of Cl^+ with respect to β are shown. (c) The ground state phase diagram in the β-α plane.

$$\begin{aligned}Cl^- &= \frac{1}{N}\sum_{n=1}^{N}\langle (S_n^x S_{n+2}^y - S_n^y S_{n+2}^x)\ S_{n+1}^z\rangle, \\ &= -\frac{1}{2N}\sum_{k\in\Lambda}\sin(2k), \\ Cl^+ &= \frac{1}{N}\sum_{n=1}^{N}\langle (S_n^x S_{n+2}^y + S_n^y S_{n+2}^x)\ S_{n+1}^z\rangle, \\ &= \frac{1}{4N}\sum_{k\in\Lambda}\sin(2k)\sin(2\theta_k) \\ &- \frac{1}{4N}\sum_{k\notin\Lambda}\sin(2k)\sin(2\theta_k). \end{aligned} \tag{20}$$

The cluster order parameter Cl^- is also referred to as the scalar chirality parameter [44]. A non-zero value of Cl^- indicates the presence of chiral ordering. The chiral order parameter serves as a measure of the helical spin alignment along a chain. In spin-1/2 chain models, chiral order can originate from various sources, including competing interactions. These chiral fluctuations play a crucial role in inducing quantum phase transitions between different chiral states or between chiral and non-chiral states. Importantly, a chiral phase is marked by the breaking of time-reversal and parity symmetries without the emergence of magnetic order.

The cluster order parameter Cl^+ is likely associated with spin nematicity [45–48]. The quantum spin-nematic phase is a unique state of matter characterized by spins in a chain aligning in two distinct directions, diverging from the typical single direction. It quantifies the extent of spin quadrupolar order within a system, where spins are oriented along two perpendicular axes instead of a singular axis.

The results for the cluster order parameters are depicted in Fig. 2 (a) and (b) for a chain size of $N = 1000$ and $\alpha = 1.0$. As shown in Fig. 2 (a), Cl^- acts as an order parameter. In the region where $\beta < \beta_c = -1.0$, the ground state exhibits chiral phase characteristics with a non-zero chirality value. Conversely, as the system transitions to the region where $\beta > \beta_c = -1.0$, the chirality vanishes. Thus, chiral ordering is present in the region $\beta < \beta_c$, and the spectrum remains gapless.

On the other hand, Fig. 2 (b) shows that Cl^+ only vanishes at $\beta = \beta_c = -1.0$, indicating no spin-nematicity at the quantum critical point. In the gapless region $\beta < \beta_c = -1.0$, Cl^+ has a small domain and changes very smoothly with varying β. However, in the next gapless region, $\beta > \beta_c = -1.0$, its value changes significantly with β. Additionally, as observed in the inset, the first derivative of Cl^+ signals the quantum critical point at $\beta = \beta_c = -1.0$. This signal at the critical point indicates a change in the slope of the order parameter Cl^+, reflecting a change in the nature of the ground state. Therefore, we can conclude that the cluster order parameter Cl^+ behaves differently in the two regions, and that a second-order quantum phase transition occurs between two types of spin-nematic ordering, namely spin-nematic-I and spin-nematic-II.

Finally, we have plotted the ground state phase diagram in Fig. 2 (c). There is a second-order quantum critical line that separates two gapless regions. In the region where $\beta < \beta_c$, a composite phase exists with long-range chiral ordering and spin-nematic-I ordering. Conversely, in the region where $\beta > \beta_c$, there is only a single gapless phase characterized by long-range spin-nematic-II ordering.

B. Concurrence and Quantum Discord

Quantum correlations are the non-classical correlations that arise between parts of a quantum system due to the principles of quantum mechanics [49–54]. These correlations are fundamentally different from classical correla-

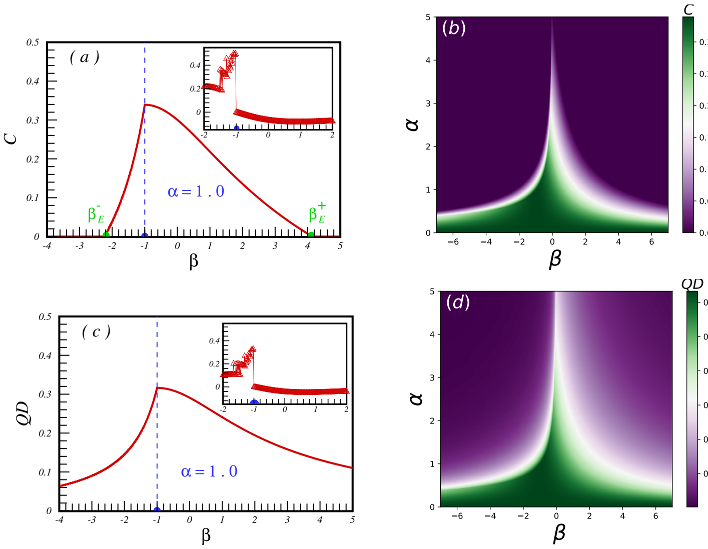

FIG. 3. (color online) (a) The concurrence as a function of β at $\alpha = 1.0$ for a chain system with $N = 1000$ particles. The inset shows the first derivative of concurrence with respect to β. (b) The density plot of concurrence in the β-α plane. (c) The QD as a function of β at $\alpha = 1.0$ for a chain system with $N = 1000$ particles. The inset shows the first derivative of QD with respect to β. (d) The density plot of QD in the β-α plane.

tions and can exhibit unique properties such as entanglement and quantum discord (QD).

When particles become entangled, their quantum states are interdependent, meaning the state of one particle cannot be described independently of the state of the other. This leads to strong correlations between the particles, even when they are separated by large distances.

A widely used method to quantify entanglement is concurrence, applicable to both pure and mixed states of two qubits [55]. Concurrence ranges from zero for separable states to one for maximally entangled states. For two arbitrary spins at positions i and j, the two-site reduced density matrix typically takes the form,

$$\rho_{ij} = \frac{1}{4} + \sum_{\mu}(\langle S_i^\mu \rangle S_i^\mu + \langle S_j^\mu \rangle S_j^\mu) + \sum_{\mu,\nu} \langle S_i^\mu S_j^\nu \rangle S_i^\mu S_j^\nu, \tag{21}$$

where $\mu, \nu = x, y, z$. The concurrence between two spin-1/2 particles at sites i and j can be derived from the corresponding reduced density matrix ρ_{ij}. The reduced density matrix in the standard basis $(|\uparrow\uparrow\rangle, |\uparrow\downarrow\rangle, |\downarrow\uparrow\rangle, |\downarrow\downarrow\rangle)$ is expressed as

$$\rho_{ij} = \begin{pmatrix} \langle p_i^\uparrow p_j^\uparrow \rangle & \langle p_i^\uparrow S_j^- \rangle & \langle S_i^- p_j^\uparrow \rangle & \langle S_i^- S_j^- \rangle \\ \langle p_i^\uparrow S_j^+ \rangle & \langle p_i^\uparrow p_j^\downarrow \rangle & \langle S_i^- S_j^+ \rangle & \langle S_i^- p_j^\downarrow \rangle \\ \langle S_i^+ p_j^\uparrow \rangle & \langle S_i^+ S_j^- \rangle & \langle p_i^\downarrow p_j^\uparrow \rangle & \langle p_i^\downarrow S_j^- \rangle \\ \langle S_i^+ S_j^+ \rangle & \langle S_i^+ p_j^\downarrow \rangle & \langle p_i^\downarrow S_j^+ \rangle & \langle p_i^\downarrow p_j^\downarrow \rangle \end{pmatrix}, \tag{22}$$

where the brackets denote the physical state average, and $p^{\uparrow} = \frac{1}{2} + S^z$, $p^{\downarrow} = \frac{1}{2} - S^z$, $S^{\pm} = S^x \pm iS^y$. The concurrence between two spins is given by $C = \max(0, \lambda_1 - \lambda_2 - \lambda_3 - \lambda_4)$, where λ_i is the square root of the eigenvalue of $R = \rho_{ij}\tilde{\rho}_{ij}$ and $\tilde{\rho}_{ij} = (\sigma_i^y \otimes \sigma_j^y)\rho_{ij}^{\star}(\sigma_i^y \otimes \sigma_j^y)$.

Due to the symmetry of the Hamiltonian, most off-diagonal elements of the reduced density matrix ρ_{ij} will be zero. First, translation invariance requires that the density matrix satisfies $\rho_{ij} = \rho_{i,i+r}$ for any position i. Additionally, our model is invariant under π-rotation around the z direction. Following these symmetry properties, the density matrix must be symmetrical, and only certain elements of the reduced density matrix become non-zero,

$$\rho_{ij} = \begin{pmatrix} X_{i,j}^{+} & 0 & 0 & F_{i,j}^{*} \\ 0 & Y_{i,j}^{+} & Z_{i,j}^{*} & 0 \\ 0 & Z_{i,j} & Y_{i,j}^{-} & 0 \\ F_{i,j} & 0 & 0 & X_{i,j}^{-} \end{pmatrix}. \tag{23}$$

Finally, the concurrence is given by

$$\begin{aligned} C &= \max\{0, C_1, C_2\}, \rangle, \\ C_1 &= 2(|Z_{i,j}| - \sqrt{X_{i,j}^{+}X_{i,j}^{-}}), \\ C_2 &= 2(|F_{i,j}| - \sqrt{Y_{i,j}^{+}Y_{i,j}^{-}}). \end{aligned} \tag{24}$$

It is important to note that the elements of the reduced density matrix for nearest-neighbor spin pairs are obtained as

$$\begin{aligned} X_{n,n+1}^{+} &= f_0^2 - |f_1|^2 + |f_2|^2, \\ X_{n,n+1}^{-} &= 1 - 2f_0 + X_{n,n+1}^{+}, \\ Y_{n,n+1}^{+} &= Y_{n,n+1}^{-} = f_0 - X_{n,n+1}^{+}, \\ Z_{n,n+1} &= f_1, \\ F_{n,n+1} &= f_2, \end{aligned} \tag{25}$$

where

$$\begin{aligned} f_0 &= \frac{1}{N}\sum_{k\in\Lambda}\cos^2(\theta_k), \qquad \varepsilon(k) < 0 \\ &= \frac{1}{N}\sum_{k\notin\Lambda}\sin^2(\theta_k), \qquad \varepsilon(k) > 0 \\ f_1 &= \frac{1}{N}\sum_{k\in\Lambda}[\cos(k)\cos^2(\theta_k) - i\sin(k)], \qquad \varepsilon(k) < 0 \\ &= \frac{1}{N}\sum_{k\notin\Lambda}\cos(k)\sin^2(\theta_k), \qquad \varepsilon(k) > 0 \\ f_2 &= -\frac{i}{2N}\sum_{k\in\Lambda}\sin(2\theta_k)\sin(k), \qquad \varepsilon(k) < 0 \\ &= \frac{i}{2N}\sum_{k\notin\Lambda}\sin(2\theta_k)\sin(k), \qquad \varepsilon(k) > 0. \end{aligned} \tag{26}$$

QD is a measure of non-classical correlations between two subsystems of a quantum system [56]. Unlike entanglement, which only captures a specific type of quantum correlation, QD includes all types of quantum correlations, even those present in separable (non-entangled) states. QD is defined as the difference between two expressions of mutual information in a quantum system. In classical information theory, mutual information is a measure of the total correlations between two systems. However, in the quantum realm, there are two different ways to generalize this concept, leading to the definition of QD.

Mathematically, for a two particles the QD is given by:

$$QD = I(\rho_{ij}) - J(i|j), \tag{27}$$

where, $I(\rho_{ij})$ is the total mutual information, defined as:

$$I(\rho_{ij}) = S(\rho_i) + S(\rho_j) - S(\rho_{ij}). \tag{28}$$

Here, $S(\rho)$ denotes the von Neumann entropy of the state ρ. $J(i|j)$ represents the classical correlations, defined as:

$$J(i|j) = S(\rho_i) - \min_{\Pi_m^j}\sum_m p_m S(\rho_{i|\Pi_m^j}), \tag{29}$$

where Π_m^j is a set of projective measurements on subsystem j, and p_m is the probability of outcome m.

We have calculated the concurrence and QD between nearest neighbor spin pairs, with the results presented in Fig. 3 (a) and (c). A chain size of $N = 1000$ and $\alpha = 1$ were considered. At the quantum critical point, $\beta_c = -1$, both concurrence and QD reach their maximum values. Additionally, as shown in the insets of Fig. 3 (a) and (c), the first derivatives of these quantities with respect to β exhibit a jump at the quantum critical point. This jump indicates a significant change in the system's quantum correlation properties and can signal a second-order quantum phase transition. In such transitions, the first derivative of the order parameter (such as concurrence) with respect to the control parameter is continuous, while the second derivative is discontinuous. The observed fluctuations in the region where $\beta < \beta_c$ are due to the size effect on the first derivatives.

Interestingly, Fig. 3 (a) reveals two entangled points in two gapless phases, which we denote as $\beta_E^{\pm}$. In the gapless composite phase with chiral and spin-nematic-I orderings, nearest-neighbor spin pairs are not entangled as $\beta \longrightarrow -\infty$. As β increases, these spin pairs remain unentangled until the entangled anisotropy β_E^{-} is reached. Beyond this point, as anisotropy increases further, the nearest-neighbor spin pairs become entangled, and concurrence rapidly grows until the quantum critical point, β_c. Conversely, in the gapless spin-nematic-II phase, no entanglement is observed between nearest-neighbor spin pairs for $\beta > \beta_E^{+}$. However, as soon as the anisotropy decreases from β_E^{+}, entanglement is created between these spin pairs. This entanglement increases gradually with decreasing β, reaching its maximum at the quantum critical point.

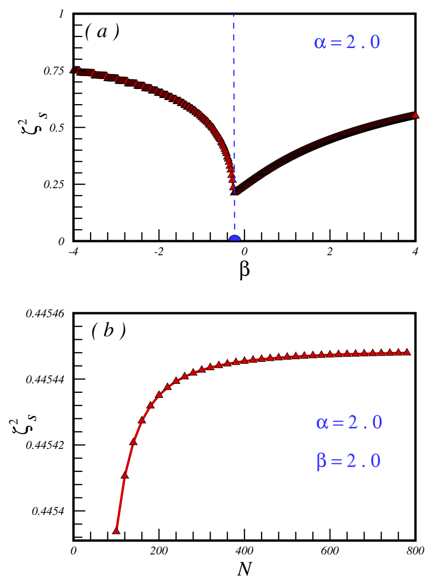

FIG. 4. (color online) (a) The behavior of the SSP as a function of β at $\alpha = 2.0$ for a chain system with $N = 1000$ particles. (b) The SSP as a function of the chain size N at $\alpha = 2.0$ and $\beta = 2.0 > \beta_c$.

The entangled region is significant for several reasons. In quantum information science, entanglement is a crucial resource for quantum computing, allowing quantum bits (qubits) to perform complex computations more efficiently than classical bits. Entangled states are also utilized in quantum communication protocols, such as quantum key distribution, which provides secure communication channels that are theoretically immune to eavesdropping. Additionally, entanglement enhances the precision of measurements in quantum sensing and imaging technologies, leading to applications in high-resolution medical imaging. Understanding entanglement in condensed matter systems can also pave the way for developing new materials with unique properties, such as high-temperature superconductors.

Fig. 3 (b) and (d) present the density plots of concurrence and QD as functions of α and β for a chain size of $N = 1000$. In both plots, the critical line defined by $\beta = -1/\alpha^2$ is clearly observed, indicating the boundary between different quantum phases. Additionally, it is evident that as α increases, the width of the entangled region decreases. This suggests that the range of β values over which nearest-neighbor spin pairs remain entangled becomes narrower with increasing α. This behavior highlights the sensitivity of the entangled region to changes in the system's parameters, providing deeper insights into the interplay between α and β in determining the entanglement properties of the system.

C. The spin squeezing and entanglement entropy

Spin squeezing is a quantum phenomenon that reduces the variance of one component of angular momentum in a collection of spin particles [57–60]. This reduction creates spin-squeezed states, which are highly valuable in quantum metrology and quantum information science. These states can improve measurement precision beyond the standard quantum limit, making them particularly useful for tasks like estimating rotation angles more accurately than classical interferometers. Additionally, spin squeezing plays a crucial role in quantum phase transitions [61–73].

To quantify spin squeezing, we use the spin squeezing parameter (SSP), which provides a measure of the degree of squeezing in the system. The SSP, denoted as ξ_s^2 and is defined as [57 and 73]

$$\xi_s^2 = \frac{2}{N}\Big[\big\langle J_x^2 + J_y^2\big\rangle - \sqrt{\big\langle J_x^2 - J_y^2\big\rangle^2 + \langle J_xJ_y + J_yJ_x\rangle^2}\Big], \tag{30}$$

where $J_\nu = \sum_{n=1}^{N} S_n^\nu$ for $\nu = x, y, z$ are total spin operators. A state is considered spin-squeezed if $\xi_s^2 < 1$. This condition indicates that the variance in one component of the angular momentum is reduced below the standard quantum limit, signifying the presence of quantum entanglement among the particles. Additionally, $\xi_s^2 = 1$ corresponds to a coherent state, which represents a minimal uncertainty state, exhibiting maximum coherence and classical behavior.

In Fig. 4, we present our findings for the SSP. In Fig. 4 (a), the SSP is plotted against the anisotropy parameter β for a chain size of $N = 1000$ and $\alpha = 2$. It is evident that the ground state of the system exhibits squeezing across the entire range of the ground state phase diagram. Notably, at the critical point $\beta_c = 0.25$, the ground state becomes extremely squeezed, and a distinct signal is observed. This indicates a significant change in the quantum correlations at the critical point.

Furthermore, in the gapless spin-nematic-II phase, where $\beta > \beta_c$, the ground state shows even more pronounced squeezing compared to the composite phase region where $\beta < \beta_c$. This increased squeezing in the gapless phase suggests stronger quantum correlations and entanglement in this region. The behavior of the SSP across different phases provides valuable insights into the nature of quantum correlations and the entanglement structure in the system, highlighting the critical role of anisotropy in determining the ground state properties. These findings contribute to a deeper understanding of the quantum phase transitions and the entanglement characteristics in spin-1/2 chains.

In the following section, we explore how the SSP changes with variations in system size. Investigating the scaling behavior of SSP is essential for several reasons. By analyzing the scaling behavior of SSP, we can gain a deeper understanding of quantum phase transitions and the associated critical phenomena. Additionally, examining SSP's scaling behavior can enhance quantum sensors and measurement devices, achieving higher precision close to the Heisenberg limit.

In the field of quantum metrology and quantum sensing, the precision of quantum measurements in spin systems is determined by two fundamental limits: the standard limit and the Heisenberg limit. The standard limit, also known as the shot-noise limit or standard quantum limit, defines the precision achievable with uncorrelated or coherent spin states [74 and 75]. This limit scales as $\zeta_s \propto 1/\sqrt{N}$, where N represents the number of spins. Essentially, as the number of spins increases, the precision improves, but only up to a certain point dictated by this limit.

In contrast, the Heisenberg limit, also referred to as the ultimate limit or quantum Cramér-Rao bound, represents the precision attainable with entangled or squeezed spin states. This limit scales as $\zeta_s \propto 1/N$ [76–78], indicating a much higher precision compared to the standard limit. The Heisenberg limit sets the highest possible precision achievable by any quantum state, surpassing the standard limit by a factor of $1/\sqrt{N}$. This means that for a large number of spins, the precision at the Heisenberg limit is significantly better than at the standard limit.

We present our scaling results in Fig. 4 (b). It is important to note that we observed scaling behavior only in the gapless region where $\beta > \beta_c$. Therefore, the results in this figure are provided for $\alpha = 2.0$ and $\beta = 2.0 > \beta_c = 0.25$. As illustrated in Fig. 4 (b), the SSP scales as $\zeta_s^2 = a + b/N^2$.

Surprisingly, we found that in the gapless spin-nematic-II phase, the Heisenberg limit can be achieved. This is a significant finding as it suggests that the system exhibits a high degree of quantum correlations, allowing for precision measurements that approach the ultimate quantum limit. Achieving the Heisenberg limit in this phase implies that the system can be used for highly sensitive quantum sensing and metrology applications, where the precision of measurements is crucial. This result highlights the potential of the gapless spin-nematic-II phase for practical applications in quantum technologies, making it an exciting area for further research and exploration.

Spin squeezing and entanglement entropy (EE) [79] are closely related concepts in quantum mechanics and both of them are invaluable tools for studying the ground state phase diagram of quantum systems. EE measures the degree of quantum entanglement between two subsystems of a composite quantum system. It quantifies the information loss or inaccessibility when only one of the subsystems is accessible, rather than the entire system.

EE is crucial in studying the ground state phase diagram because it provides deep insights into the quantum entanglement properties of a system. By measuring the degree of entanglement between different parts of a system, EE helps identify and characterize quantum phase transitions and critical points. Changes in EE can signal different quantum phases and their boundaries, offering a clear picture of the underlying quantum phenomena. This makes EE a powerful tool for understanding the complex behavior of quantum systems and mapping out their ground state phase diagrams.

One common method to define EE involves the density operator and calculating the von Neumann entropy of a reduced density matrix for a subsystem [80 and 81]. For a bipartite system, the EE is defined as the von Neumann entropy of subsystem A:

$$S_A = -\mathbf{Tr}[\rho_{\mathbf{A}} \log_{\mathbf{2}}(\rho_{\mathbf{A}})], \tag{31}$$

where ρ_A is the reduced density matrix of A, obtained by tracing over the rest of the system, B:

$$\rho_A = \mathbf{Tr}_{\mathbf{B}}(\rho). \tag{32}$$

EE typically scales with the boundary area of subsystem A, rather than its volume. This behavior, known as the 'area law' for EE, has been extensively studied. In noncritical ground states of spin chains with a finite correlation length, the EE remains constant. However, at a quantum critical point, when subsystem A is a finite interval of length l, the EE deviates slightly from the area law due to a logarithmic correction:

$$S_A(l) \sim \frac{c_{eff}}{3} \log(l), \tag{33}$$

where c_{eff} represents the central charge [82–84].

To gain deeper insights into the various gapless phases of the system, we calculated the EE in chain systems with different Hamiltonian parameters. We divided the system into two equal parts, where $N_A = N_B = \frac{N}{2}$. The results are presented in Fig. 5 for $N = 1000$ and $\alpha = 1$. As shown in Fig. 5 (a), in the composite gapless phase where $\beta < \beta_c = -1$, the EE is very large and increases rapidly as we move away from the critical point. In contrast, in the other gapless region where $\beta > \beta_c = -1$, the two equal parts are weakly entangled compared to the composite gapless phase, and the EE remains almost constant with respect to β. It is important to note that the EE reaches its minimum value at the critical point $\beta = \beta_c = -1$.

This behavior highlights the distinct entanglement properties in different gapless phases and underscores the critical point as a unique feature where the entanglement entropy is minimized. These findings provide valuable information about the quantum correlations present in the system and can help in understanding the nature of the gapless phases more comprehensively.

In the final step, we examined the scaling behavior of EE with respect to the system size. This analysis is crucial for several reasons. Firstly, it serves as a powerful tool to differentiate between various quantum phases. At critical points, EE often displays unique scaling properties that are distinct from those in bulk phases. By investigating how EE scales with system size, researchers can gain valuable insights into the distribution and strength

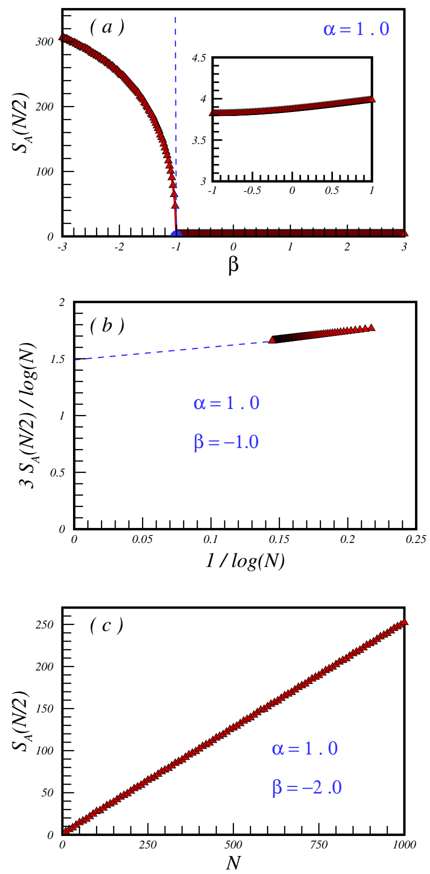

FIG. 5. (color online) (a) The EE as a function of β at $\alpha = 1.0$ for a chain with $N = 1000$ particles. (b) A linear fit of the form $Y = mX + b$ applied to the function $3S_A(N/2)/\log(N) = c_{eff} + m/\log(N)$ on the critical line $\beta_c = -1.0$ at $\alpha = 1.0$. (c) The EE in the gapless composite phase as a function of the chain size N.

of quantum correlations in the ground state, which is particularly important for understanding the entanglement structure in strongly correlated systems. Additionally, the scaling of EE has significant implications for the efficiency of classical simulations of quantum systems. Systems exhibiting area law scaling of EE can often be efficiently simulated using tensor network methods, such as matrix product states, whereas systems with volume law scaling of EE are generally more challenging to simulate classically. Overall, studying the scaling of EE in spin-1/2 chain systems provides a deep understanding of the quantum properties and phase structure of these systems, making it a vital aspect of modern condensed matter physics and quantum information science. Results are presented in Fig. 5 (b) and (c).

Fig. 5 (b) presents the results when the system is at the quantum critical point $\beta = \beta_c = -1$. Our findings reveal that the central charge in this scenario is $c_{\text{eff}} = 1.5$. We conducted similar calculations for all critical points along the critical line $\beta_c = -\frac{1}{\alpha^2}$ and consistently found the same central charge. Different values of the central charge indicate distinct critical behaviors and symmetries of the system at these points. For instance, a central charge of 0.5 is often linked to systems like the transverse field Ising model at criticality, 1.0 is typical for the isotropic XX spin-1/2 chain, and 1.5 suggests more complex critical behavior, potentially indicating the presence of multiple degrees of freedom or more intricate topological features. Additionally, we observed that when the system is in the gapless spin-nematic-II phase, $\beta > \beta_c$, the logarithmic behavior with a central charge of $c_{\text{eff}} = 1.5$ indicates that this phase is also critical.

Interestingly, we have found that the EE in the gapless composite phase exhibits a completely different scaling behavior. As shown in Fig. 5 (c), EE in the region $\beta < \beta_c$ displays a linear relationship with the system size, indicating that EE is an extensive parameter and follows volume-law scaling. This contrasts with area-law scaling, where EE scales with the surface area of the system and is often associated with systems that are more challenging to simulate classically. The linear behavior of EE in our system suggests that the ground state in the gapless region $\beta < \beta_c$ exhibits extensive entanglement, which is not typical for gapped systems but can occur in critical systems or those with long-range entanglement [85].

This behavior indicates that the system has a high degree of quantum correlations spread across its entire length, rather than being localized near the boundaries. Such extensive entanglement is characteristic of systems with volume-law scaling and implies that the quantum correlations are not confined to a specific region but are distributed throughout the system. This finding is significant as it provides insights into the nature of the quantum state in the gapless composite phase, highlighting the presence of strong, long-range entanglement. Understanding this behavior is crucial for developing efficient simulation methods and for gaining a deeper comprehension of the entanglement structure in strongly correlated quantum systems.

Volume-law scaling of EE in a spin-1/2 chain has several important applications across various fields. In condensed matter physics, it helps in understanding the nature of quantum phases and phase transitions, particularly in systems with high entanglement. This scaling provides insights into the behavior of strongly correlated materials and can reveal complex topological features and multiple degrees of freedom. In quantum information science, volume-law scaling is crucial for studying quantum chaos and integrability. It aids in diagnosing the entanglement structure of quantum states, which is essential for developing efficient quantum algorithms and understanding the limits of quantum computation.

In quantum metrology, volume-law scaling can enhance the precision of measurements by exploiting the extensive entanglement in quantum systems. This is particularly useful in achieving better-than-classical precision in estimating parameters, such as magnetic fields or gravitational waves, through quantum-enhanced sensing techniques. Additionally, in quantum measurements, the study of volume-law scaling can lead to a deeper understanding of measurement-induced phase transitions. It helps in identifying the conditions under which a system transitions from volume-law to area-law entanglement, which is important for optimizing measurement protocols and improving the accuracy of quantum state tomography. These applications highlight the significance of volume-law scaling in advancing our understanding and capabilities in various domains of quantum science and technology.

IV. CONCLUSION

Our comprehensive analysis of the spin-1/2 XX chain model with anisotropic three-spin interaction has revealed a rich tapestry of ground state properties and phase behaviors. By employing the fermionization technique and exact diagonalization of the Hamiltonian, we have identified two distinct gapless phases separated by a second-order critical line. The composite phase is characterized by both chiral and spin-nematic-I long-range orderings, while the spin-nematic-II phase exhibits unique long-range ordering.

In the first part of our study, we analyzed the dispersion relation, ground state energy, fidelity susceptibility, and order parameters. These analyses allowed us to map out the phase diagram and identify the critical line separating the two gapless phases. The composite phase, with its chiral and spin-nematic-I orderings, and the spin-nematic-II phase, with its distinct ordering, highlight the complex interplay of interactions in the system.

Next, we focused on the quantum correlations between nearest-neighbor spins by examining the concurrence and QD. Our findings indicate that these measures are maximized at the critical line, underscoring the enhanced quantum correlations in this region. Additionally, we observed an entangled region, further emphasizing the intricate quantum nature of the ground state.

In the final part of our study, we investigated the SSP and EE. Our results show that the ground state is squeezed throughout the phase diagram, with extreme squeezing occurring at the critical line. Remarkably, in the gapless spin-nematic-II phase, the Heisenberg limit is achieved, indicating the potential for high-precision measurements in this phase. By dividing the system into two equal parts, we found significant entanglement in the gapless composite phase, highlighting the strong quantum correlations present.

The central charge calculation confirms the critical nature of the gapless spin-nematic-II phase, based on the scaling of the EE. Furthermore, the EE follows volume-law scaling in the gapless composite phase, indicating that it is an extensive parameter in this region.

Overall, our findings contribute to the understanding of quantum phase transitions and the role of multi-spin interactions in low-dimensional quantum systems. The identification of distinct gapless phases, critical lines, and regions of enhanced quantum correlations provides valuable insights for future research in quantum information and condensed matter physics. These results may also have implications for the development of quantum technologies, where understanding and harnessing quantum correlations and entanglement are crucial.

---

[1] A. N. Vasiliev, O. S. Volkova, E .A. Zvereva, M. M. Markina, *Low-dimensional magnetism*, CRC Press, ISBN 9781032239002 (2019).

[2] A. Vasiliev, O. Volkova, E. Zvereva and M. Markina, *Milestones of low-D quantum magnetism*, npj Quant. Mater. **3**, 18 (2018).

[3] S. Sachdev, *Quantum Phase Transitions*, 2nd ed. Cambridge University Press, (2011).

[4] Matthias Vojta, Quantum Phase Transitions, Rep. Prog. Phys. **66**, 2069 (2003).

[5] F. D. M. Haldane, Phys. Rev. Lett. **50**, 1153 (1983).

[6] A. O. Gogolin, A. A. Nersesyan and A. M. Tsvelik, *"Bosonization and strongly correlated systems"*, (Cambridge University Press 1998).

[7] T. Giamarchi, *"Quantum Physics in One Dimension"*, (Clarendon Press, Oxford 2004).

[8] M. Takahashi, *"Thermodynamics of One Dimensional Solvable Models"*, (Cambridge University Press 1998).

[9] M. Suzuki, Phys. Lett. A **34**, 91 (1971); Prog. Theor. Phys. **46**, 1337 (1971).

[10] I. Titvinidze, and G. I. Japaridze, Eur. Phys. J. B **32**, 383 (2003); Georgian, B., Natl. Acad. Sci, **163**, 501 (2004).

[11] Ping Lou, Wen-Chin Wu, and Ming-Che Chang, Phys. Rev. B **70**, 064405 (2004).

[12] J. K. Pachos, and M. B. Plenio, Phys. Rev. Lett. **93**, 056402 (2004).

[13] B. Horstmann, J. I. Cirac, and T. Roscilde, Phys. Rev. A, **76**, 043625 (2007).

[14] Oleg Derzhko, Taras Krokhmalskii, Joachim Stolze, and Taras Verkholyak, Phys. Rev. B, **79**, 094410 (2009).

[15] W. W. Cheng and J.-M. Liu, Phys. Rev. A, **80**, 012308 (2010).

[16] Y. C. Li, and H. Q. Lin, Phys. Rev. A, **83**, 052323 (2011).

[17] R. Jafari, S. Mahdavifar, Prog. of Theo. and Exp. Phys. **4**, 043I02 (2014).

[18] G. Zhang and Z. Song, Phys. Rev. Lett. **115**, 177204 (2015).

[19] Thiago M Carrijo et. al., J. Phys. B: At. Mol. Opt. Phys. **48**, 125501 (2015).

[20] Wen-Long You, Yu-Cheng Qiu, and Andrzej M. Oleś, Phys. Rev. B **93**, 214417 (2016).

[21] U. Divakaran, S. Sharma, and A. Dutta, Phys. Rev. E, **93**, 052133 (2016).

[22] M. Tahvili, and S. Mahdavifar, Physica A: Statistical Mechanics and its Applications, **466**, 21 (2017).

[23] Z. Shadman, H. Cheraghi, S. Mahdavifar, Physica A: Sta-

tistical Mechanics and its Applications, **512**, 1128 (2018).
[24] Z. Noorinezhad, B. Haghdoust, M. R. Abolhassani, M. Ilkhani, S. Mahdavifar, Journal of Superconductivity and Novel Magnetism, **32**, 3873 (2019).
[25] Ming-Liang Hu, Yun-Yue Gao, and Heng Fan, Phys. Rev. A, **101**, 032305 (2020).
[26] Shuangshuang Fu, Xiaohui Li, and Shunlong Luo, Phys. Rev. A, **106**, 062405 (2022).
[27] M. Khastehdel Fumani, S. Mahdavifar, K. Afrousheh, Phys. Rev. E **109**, 044142 (2024).
[28] David Gottlieb and Jaime Rossler, *Exact solution of a spin chain with binary and ternary interactions of Dzialoshinsky-Moriya type*, Phys. Rev. B **60**, 9232 (1999).
[29] Ping Lou, Wen-Chin Wu, and Ming-Che Chang *Quantum phase transition in spin-12 XX Heisenberg chain with three-spin interaction*, Phys. Rev. B **70**, 064405 (2004).
[30] M. Topilko, T. Krokhmalskii, O. Derzhko,a, and V. Ohanyan, *Magnetocaloric effect in spin-1/2 XX chains with three-spin interactions*, Eur. Phys. J. B **85**, 278 (2012).
[31] Xiaoxian Liu et. al. *Chiral phase and quantum phase transitions of anisotropic XY chains with three-site interactions*, J. Stat. Mech. **01**, P01003 (2012); Xiaoxian Liu et. al. *Erratum: Chiral phase and quantum phase transitions of anisotropic XY chains with three-site interactions*, J. Stat. Mech. **11**, E11001 (2012).
[32] Shuguo Lei, Peiqing Tong, *Quantum discord in the transverse field XY chains with three-spin interaction*, Physica B **463**, 1-6 (2015).
[33] Ming-Liang Hu, Yun-Yue Gao, and Heng Fan, *Steered quantum coherence as a signature of quantum phase transitions in spin chains*, Phys. Rev. A **101**, 032305 (2020).
[34] P. Thakur, P. Durganandini, *Orbital antiferroelectricity and higher dimensional magnetoelectric order in the spin-1/2 XX chain extended with three-spin interactions*, Eur. Phys. J. B **96**, 51 (2023).
[35] S. Mahdavifar, B. Haghdoost, F. Khastehdel Fumani, M. R. Soltani, Quantum Information Processing, **23**, 284 (2024).
[36] Y. Wang, B. B. Chai, JL. Guo, Int. J. Theor. Phys. **57**, 2504 (2018).
[37] Hannes Weisbrich, Wolfgang Belzig and Gianluca Rastelli, SciPost Phys. **6**, 037 (2019).
[38] Lin-Lin Su, Jun Ren, Wen-Long Ma, Z. D. Wang, and Yan-Kui Bai, Phys. Rev. B **110**, 104101 (2024).
[39] S. Mahdavifar, F. Khastehdel Fumani, H. Cheraghi, Submitted.
[40] Ming-Ming Du, Shi-Pu Gu, Wei Zhong, Xiao-Jing Yan, Lan Zhou, Yu-Bo Sheng, Annalen der Physik, **535** 8 (2023).
[41] S.-J. Gu, Int. J. Mod. Phys. B, **24** 4371 (2010).
[42] S.-J. Gu, Phys. Rev. E, **79** 061125 (2019).
[43] S.-J. Gu and H.-Q. Lin, Europhys. Lett. **87** 10003 (2019).
[44] G. Wen, F. Wilczek, and A. Zee, Phys. Rev. B **39** 11413 (1989).
[45] R. Mao, Y.-W. Dai, S. Y. Cho, and H.-Q. Zhou, Phys. Rev. B **103**, 014446 (2021).
[46] W. Yang, A. Nocera, E. S. Srensen, H.-Y. Kee and I. Affleck, Phys. Rev. B **103**, 054437 (2021).
[47] S. Mahdavifar, D. C. Liu, Sci. Rep. **14**, 30024 (2024).
[48] M. Abbasi, S. Mahdavifar, M. Motamedifar, Scipost phys. core. **8**, 001 (2025).
[49] A. Osterloh, L. Amico, G. Falci, R. Fazio, Nature **416**, 608 (2002); L. Amico, R. Fazio, A. Osterloh and V. Vedal, Rev. Mod. Phys. **80**, 517 (2008).
[50] R. Horodecki, P. Horodecki, M. Horodecki and K. Horodecki, Rev. Mod. Phys. **81**, 865 (2009).
[51] N. Loflorence, Physics Report **646**, 1-59 (2016).
[52] A. Bera, T. Das, D. Sadhukhan, S. S. Roy, A. Sen and U. Sen , Rep. Prog. Phys. **81**, 024001 (2018).
[53] D. Braun, G. Adesso, F. Benatti, R. Floreanini, U. Marzolino, M. W. Mitchell, S. Pirandola, Rev. Mod. Phys. **90**, 35006 (2018).
[54] Anindita Bera, Tamoghna Das, Debasis Sadhukhan, Sudipto Singha Roy, Aditi Sen(De) and Ujjwal Sen, Rep. Prog. Phys. **81**, 024001 (2018).
[55] W. K. Wootters, Phys. Rev. Lett. **80**, 2245 (1998).
[56] H. Ollivier, W. H. Zurek, Phys. Rev. Lett. **88**, 017901 (2001).
[57] J. M. Radcliffe, J. Phys. A: Gen. Phys. **4**, 313 (1971).
[58] M. Kitagawa, and M. Ueda, Phys. Rev. A **47**, 5138 (1993).
[59] D. J. Wineland, J. J. Bollinger, W. M. Itano, F. L. Moore, D. J. Heinzen, Phys. Rev. A **46**, R6797 (1992); D. J. Wineland, J. J. Bollinger, W. M. Itano, and D. J. Heinzen, Phys. Rev. A **50**, 67 (1994).
[60] For a review, see J. Ma, X. Wang, C. P. Sun, and F. Nori, Phys. Rep. **509**, 89 (2011).
[61] J. Vidal, G. Palacios, and R. Mosseri, Phys. Rev. A **69**, 022107 (2004).
[62] W-F. Liu, J. Ma and X. Wang, J. Phys. A: Math. Theor. **46**, 045302 (2013).
[63] S. Dusuel and J. Vidal, Phys. Rev. Lett. **93**, 237204 (2004).
[64] J. Ma and X. Wang, Phys. Rev. A **80**, 012318 (2009).
[65] L. Pezze, A. Smerzi, M. K. Oberthaler, R. Schmied, and P. Treutlein, Rev. Mod. Phys. **90**, 035005 (2018).
[66] I. Frerot, T. Roscilde, Phys. Rev. Lett. **121**, 020402 (2018).
[67] V. Makhalov, T. Satoor, A. Evrard, T. Chalopin, R. Lopes, and S. Nascimbene, Phys. Rev. Lett. **123**, 120601 (2019).
[68] H. Bao, J. Duan, S. Jin, X. Lu, P. Li, W. Qu, M. Wang, I. Novikova, E. E. Mikhailov, K-F. Zhao, K. Mølmer, H. Shen, Y. Xiao, Nature **581**, 159 (2020).
[69] K. Hayashida, T. Makihara, N. M. Peraca, D. F. Padilla, H. Pu, J. Kono, M. Bamba, Scientific Reports **13**, 2526 (2023).
[70] I. Frérot, M. Fadel, M. Lewenstein, Rep. Prog. Phys. **86** 114001 (2023).
[71] L. Xin, M. Barrios, J. T. Cohen, M. S. Chapman, Phys. Rev. Lett. **131**, 133402 (2023).
[72] S. Mahdavifar, M. Salehpour, H. Cheraghi, K. Afrousheh, Sci. Rep. **14**, 10034 (2024).
[73] H. Cheraghi, S. Mahdavifar, H. Johannesson, Phys. Rev. B **105** 024425, (2022).
[74] S. F. Huelga, et al. Phys. Rev. Lett. **79**, 3865 (1997).
[75] B. M. Escher, R. L. de Matos Filho, L. Davidovich, Nat. Phys. **7**, 406 (2011).
[76] V. Giovannetti, S. Lloyd, L. Maccone, Science **306**, 1330 (2004).
[77] V. Giovannetti, S. Lloyd, L. Maccone, Nat. Photonics **5**, 222 (2011).
[78] E. Davis, G. Bentsen, M. Schleier-Smith, Phys. Rev. Lett. **116**, 053601 (2016).
[79] C. H. Bennett, H. J. Bernstein, S. Popescu, and B. Schumacher, Phys. Rev. A **53**, 2046 (1996).
[80] A. Kitaev and J. Preskill, Phys. Rev. Lett. **96**, 0110404

(2006).
[81] A. Bergschneider, V. M. Klinkhamer, J. H. Becher, R. Klemt, L. Palm, G. Zurn, S. Jochim, and P. M. Preiss, Nature Physics **15**, 640 (2019).
[82] P. Calabrese and J. Cardy, J. Stat. Mech. **06**, P06002 (2004).
[83] M. B. Hastings, J. Stat. Mech. **08**, P0802 (2007).
[84] J. Eisert, M. Cramer, M.B. Plenio, Rev. Mod. Phys. **828**, 277 (2010).
[85] G. Vitagliano, A. Riera, and J. I. Latorre, New Journal of Physics **12**, 113049 (2010).